J Biol Inorg Chem (2006) 11: 197–205
DOI 10.1007/s00775-005-0066-5

ORIGINAL PAPER

Benjamin F. Gherman · David E. Heppner
William B. Tolman · Christopher J. Cramer

Models for dioxygen activation by the Cu_B site of dopamine β-monooxygenase and peptidylglycine α-hydroxylating monooxygenase

Received: 10 August 2005 / Accepted: 21 November 2005 / Published online: 13 December 2005

Abstract On the basis of spectroscopic and crystallographic data for dopamine β-monooxygenase and peptidylglycine α-hydroxylating monooxygenase (PHM), a variety of ligand sets have been used to model the oxygen-binding Cu site in these enzymes. Calculations which employed a combination of density functional and multireference second-order perturbation theory methods provided insights into the optimal ligand set for supporting η^1 superoxo coordination as seen in a crystal structure of a precatalytic Cu/O_2 complex for PHM (Prigge et al. in *Science* 304:864–867, 2004). Anionic ligand sets stabilized η^2 dioxygen coordination and were found to lead to more peroxo-like $Cu–O_2$ complexes with relatively exergonic binding free energies, suggesting that these adducts may be unreactive towards substrates. Neutral ligand sets (including a set of two imidazoles and a thioether), on the other hand, energetically favored η^1 dioxygen coordination and exhibited limited dioxygen reduction. Binding free energies for the 1:1 adducts with Cu supported by the neutral ligand sets were also higher than with their anionic counterparts. Deviations between the geometry and energetics of the most analogous models and the PHM crystal structures suggest that the protein environment influences the coordination geometry at the Cu_B site and increases the lability of water bound to the preoxygenated reduced form. Another implication is that a neutral ligand set will be critical in biomimetic models in order to stabilize η^1 dioxygen coordination.

Keywords Density functional theory · Copper peroxide · Copper superoxide · Dopamine β-monooxygenase · Peptidylglycine α-hydroxylating monooxygenase

Introduction

The Cu-containing enzymes dopamine β-monooxygenase (DβM) [1, 2] and peptidylglycine α-hydroxylating monooxygenase (PHM) [1, 3, 4] play central roles in neurobiology by regulating levels of neurohormones. These enzymes exhibit substantial functional and structural similarities. The first step in each of their respective catalytic cycles involves the binding and activation of molecular oxygen, after which substrate C–H bond oxidation occurs, resulting in the conversion of dopamine to norepinephrine in the case of DβM and α-hydroxylation of glycine-extended peptides in the case of PHM. In addition to the 32% sequence identity in the two enzymes [5, 6], active-site residues are also conserved between them, which has been taken to imply analogous catalytic mechanisms in each system [1, 7–10]. Both enzymes contain two noncoupled Cu active sites, denoted Cu_A (or Cu_H) and Cu_B (or Cu_M), separated by about 10 Å [10, 11]. The two metal atoms are not linked by any bridging ligands and cycle through Cu(I) and Cu(II) oxidation states during catalysis. Cu_A is believed to function principally as an electron transfer site, while Cu_B is the site at which dioxygen binding and subsequent substrate hydroxylation take place.

Among recent work examining dioxygen–copper systems [12–14], the activation of molecular oxygen at the Cu_B site has in particular been probed via crystallographic studies and the use of biomimetic models. Chen et al. [15, 16] have used theory to model both a side-on (η^2) bound 1:1 Cu_B/O_2 adduct and hydroperoxo intermediates using crystal structures of the PHM catalytic core [10] to generate starting geometries. Among the many biomimetic models for DβM and PHM in the literature [17–22], those of Tolman and coworkers

Electronic Supplementary Material Supplementary material is available for this article at http://dx.doi.org/10.1007/s00775-005-0066-5 and is accessible for authorized users.

B. F. Gherman (✉) · D. E. Heppner · W. B. Tolman
C. J. Cramer
Department of Chemistry and Supercomputer Institute,
University of Minnesota, 207 Pleasant St. SE,
Minneapolis, MN 55455, USA
E-mail: gherman@pollux.chem.umn.edu
Fax: +1-612-6262006

[23–25] are among the most thoroughly investigated. Using β-diketiminate and anilido-imine ligands, they have isolated 1:1 side-on Cu–O_2 adducts and characterized them both experimentally and theoretically. However, these Cu–dioxygen model complexes proved to be unreactive towards substrates in potential hydroxylation reactions [26]. Moreover, a crystal structure of a precatalytic complex of PHM with a bound, inactive substrate analog has shown not only that dioxygen binds end-on (η^1) to the Cu_B site, but also that the O–O bond length in this intermediate is short enough to rule out the possibility that the complex is a peroxo or hydroperoxy intermediate [11].

Given the present disparity between current modeling efforts and the PHM Cu–O_2 crystal structure, we here examine a variety of active-site models based upon crystallographic and spectroscopic data for DβM and PHM in order to model dioxygen activation at Cu_B. By comparing the geometries, energies, and electronic structures of these different models, we will determine the influence of ligand coordination on the dioxygen binding mode and complex stability. These results provide insight into nature's choice of ligands at the Cu_B sites in DβM and PHM and provide suggestions for the design of new biomimetic model systems, which might better represent these enzymes' chemistries.

Choice of model systems

Model systems for the current study are based upon available crystallographic and spectroscopic data for DβM and PHM. Extended X-ray absorption fine structure (EXAFS) data for DβM indicate two histidine residues, a weakly bound unknown ligand (likely solvent-derived), and a Met–S coordinated to Cu_B(I) [27, 28]. In oxidized DβM, the methionine has been proposed to be weakly bound in an axial position [28]. With regard to PHM, a combined EXAFS/electron paramagnetic resonance (EPR)/Fourier transform IR study concluded that Cu_B(I) was three-coordinate, with two histidines and one methionine as ligands [29]; other EXAFS experiments suggest that Cu_B(I) could be either three- or four-coordinate [30]. The crystal structure of the reduced PHM catalytic core shows two histidines (H242 and H244), one methionine (M314), and one solvent-derived moiety ligated to Cu_B(I) [9, 10, 31]. A similar ligand environment is seen in the crystal structure of a precatalytic Cu–O_2 complex for PHM, except that a solvent-derived ligand is absent in this case [11].

Pooling these structural data suggests that realistic models should satisfy the following criteria: (1) the Cu(I) complexes should have either three or four ligands, (2) there should be at least two N-coordinating ligands, and (3) the other coordination sites should be occupied by up to one thioether group or up to two solvent-derived ligands. Based on these constraints, the following three-coordinate Cu(I) complexes are investigated: $[Cu(N)_3]^+$, $[Cu(N)_2(H_2O)]^+$, $[Cu(N)_2(OH)]$, and $[Cu(N)_2(S)]^+$, where the nitrogen donating ligand N will be imidazole in the place of a histidine residue, the solvent-derived ligand will be either water or hydroxide, and S represents dimethyl sulfide to model a methionine residue. Eight four-coordinate complexes are also potentially consistent with the structural data at hand: $[Cu(N)_3(H_2O)]^+$, $[Cu(N)_3(OH)]$, $[Cu(N)_2(H_2O)_2]^+$, $[Cu(N)_2(H_2O)(OH)]$, $[Cu(N)_2(OH)_2]^-$, $[Cu(N)_3(S)]^+$, $[Cu(N)_2(H_2O)(S)]^+$, and $[Cu(N)_2(OH)(S)]$.

Models for the PHM active site in the reduced and oxygenated forms of the enzyme were derived from available crystal structures (PDB ID codes 3PHM and 1SDW, respectively) [10, 11] by extracting coordinates for the Cu_B center, dioxygen, and coordinating side chains and solvent molecules. After adding hydrogen atoms as appropriate, all degrees of freedom were optimized except for the Cu–N, Cu–S, and Cu–O(H_2O) distances and the relative orientations of the imidazole rings. The resulting structures allow for the energetic effects of the protein-induced coordination geometries versus those seen in the more completely optimized model complexes to be determined (*vide infra*). In order to test the validity of constructing enzyme models in this manner and, in particular, the quality of the crystallographic metal–ligand bond distances, calculations were carried out in which the bond angles around the Cu center were frozen and metal–ligand bond distances were optimized. Differences in the calculated and experimental metal–ligand bond lengths in the reduced structure, which had a crystallographic resolution of 2.10 Å [10], were 0.06 Å for Cu–N and Cu–S and 0.40 Å for H_2O (which reduces to 0.08 Å if replaced with hydroxide). These differences correspond to an electronic energy difference of 8.8 kcal mol^{-1} (8.0 kcal mol^{-1} with hydroxide present) upon relaxation of the metal–ligand bond lengths. In the case of the oxygenated form of PHM, where the crystal structure was obtained at the higher resolution of 1.85 Å [11], the differences were 0.04 Å for Cu–N, 0.14 Å for Cu–S, and 0.10 Å for O_2. The concomitant difference in the O–O bond length was nominal (0.01 Å). The electronic energy decrease upon optimization of the metal–ligand bond lengths was only 2.5 kcal mol^{-1}. These data imply the metal–ligand bond distances in the crystal structures are reliable and show that the differences in the calculated and experimental structures do not significantly impact upon dioxygen activation.

Computational methods

Density functional methods

Geometry optimizations were performed using the Jaguar suite, version 5.0, of ab initio quantum chemistry programs [32]. Density functional theory (DFT) with the B3LYP functional [33–35], which has previously been shown to be successful in predicting ligand–Cu(I) and ligand–Cu(II) bond dissociation energies [36], was used

for the calculation of structures and energies. Based upon previous studies of 1:1 adducts formed from Cu(I) complexes and dioxygen [24, 25, 37], geometry optimizations were carried out using a restricted (RDFT) methodology for singlet cases and an unrestricted (UDFT) methodology for the triplet cases. The 6-31G(d,p) basis set was used for all atoms, except for Cu, for which the lacvp** basis set [38–40], which includes an effective core potential, was used. Vibrational frequencies were calculated analytically and scaled by a factor of 0.96 [41], allowing for structures to be confirmed as minima and the inclusion of zero-point-energy effects, thermal corrections to enthalpies, and entropic contributions in computed free energies of reaction.

As the active site in PHM is solvent-exposed and a solvent-filled cleft separates the Cu_A and Cu_B sites in PHM [10, 11], inclusion of solvation effects is crucial in order to obtain binding energies relevant to the biological system. The solvation free energy of dioxygen in water at 25 °C can be calculated from its Henry's Law constant to be +3.95 kcal mol^{-1} (in this work all solvation free energies refer to a standard state of 1 atm in the gas phase and 1 mol L^{-1} in solution). A standard-state correction equal to $-RT$ ln(24.47), where 24.47 is the molar volume of an ideal gas at 1 atm and 25 °C, is applied to free energies of reaction in which an adduct is formed from dioxygen and a Cu(I) complex [42]. The self-solvation free energy for water at 25 °C is −6.31 kcal mol^{-1} [43]. For those reactions in which water occurs as a product, the free energies must be corrected by $+RT$ ln(55.6) to account for the 55.6 M standard-state concentration of water [42]. As oxygenation does not change the overall charge of the Cu-containing species, the electrostatic contribution and hence the total solvation free energy (which is dominated by the electrostatic term) are virtually unaffected. Thus, differences in solvation energies between Cu(I) complexes and their oxygenated forms are assumed to be negligible and are not explicitly included in the calculated enthalpy changes for the oxygenation reactions. This assumption is likely to introduce errors no larger than those implicit in the computation of free energies of solvation for charged species [44].

A Born–Haber free-energy cycle (Scheme 1) is used to determine pK_a values. The free energy for deprotonation in aqueous solution is given by Eq. 1:

$$\Delta G_a = \Delta G_g - \Delta G_{sol}^{AH} + \Delta G_{sol}^{A-} + \Delta G_{sol}^{H+}, \quad (1)$$

where ΔG_g is the gas-phase deprotonation energy and ΔG_{sol}^{AH}, ΔG_{sol}^{A-}, and ΔG_{sol}^{H+} are the solvation free energies for the conjugate acid and base forms and the proton. Solvation free energies for HA and A^- are calculated with a self-consistent reaction field method using the Poisson–Boltzmann solver implemented in Jaguar [45, 46]. The solvation free energy for the proton is taken to be −264.0 kcal mol^{-1} [47]. The pK_a is then computed as

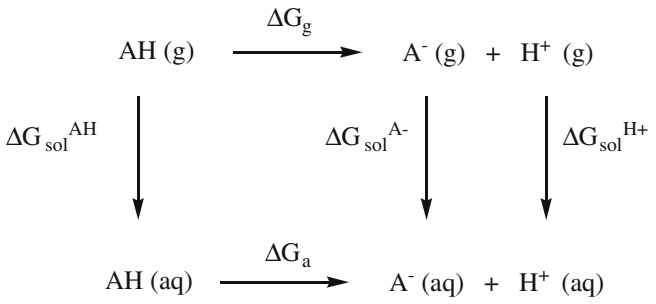

Scheme 1 Born–Haber free-energy cycle

$$pK_a = \frac{\Delta G_a}{2.303RT}, \quad (2)$$

where R is the universal gas constant and T is temperature. Empirical corrections to the calculated pK_a values were assessed in order to compensate for any systematic error introduced by the computational methodology. The oxonium ions $CH_3OH_2^+$ and $CH_3CH_2OH_2^+$ and the hydronium ion H_3O^+ can serve as model compounds for water bound to a Cu(I) site. Calculated pK_a values for these species are −2.3, −3.5, and −2.1, respectively, while experimental values are −2.1, −1.9, and −1.7 [48]. Averaging the differences between the two sets of numbers leads to a correction factor of +0.7. Similarly, imidazole bound to Cu(I) may be modeled by imidazolium. The computed pK_a of 17.8 differs from the experimental value of 7.0 [49], pointing to a correction of −10.8 units in this case.

Multireference methods

While closed-shell singlet and high-spin triplet Kohn–Sham wave functions can be expressed as single Slater determinants, open-shell singlets formally require at least two determinants and therefore are not a priori representable within the framework of Kohn–Sham DFT. Open-shell singlets are particularly relevant in Cu–O_2 adducts, however, especially those with a significant degree of Cu(II)–superoxo character, i.e., those which most resemble a biradical with one electron localized to Cu and the other to O_2. In order to account for the multideterminantal nature of the singlet adducts when calculating these species' energies and to compute accurate singlet–triplet energy differences, single-point multireference second-order perturbation theory (CASPT2) [50] calculations were carried out. The complete active space (CAS) for the reference wave functions was composed of 18 electrons and 12 orbitals and consisted of the Cu valence electrons/orbitals and the σ_{2p}, σ_{2p}*, π_{2p}, and π_{2p}* electrons/orbitals from the dioxygen moiety. After removing orbitals with occupation numbers greater than 1.999, a final (12,9) active space was arrived at (see Ref. [37] for more details). The MOLCAS program was used for all CAS and CASPT2

calculations [51]. A 17-electron relativistic effective core potential basis set was used for Cu [52] and a polarized double-zeta atomic natural orbital basis set was used for all other atoms [53].

In order to make the CASPT2 calculations more tractable, a simplified version of the models was used in which the imidazole ligands were changed to ammine ligands. The overall geometry was kept unchanged from that of the full model, except that the positions of the ammine hydrogen atoms were optimized at the DFT level prior to the CASPT2 calculations. Using this small model, differences between the singlet/triplet splittings at the DFT and CASPT2 levels of theory were calculated according to

$$\begin{aligned}\Delta &= \left({}^1\mathrm{A} - {}^3\mathrm{A}\right)_{\mathrm{CASPT2}} - \left({}^1\mathrm{A} - {}^3\mathrm{A}\right)_{\mathrm{DFT}} \\ &= \left[\left({}^1\mathrm{A}\right)_{\mathrm{CASPT2}} - \left({}^1\mathrm{A}\right)_{\mathrm{DFT}}\right] \\ &\quad - \left[\left({}^3\mathrm{A}\right)_{\mathrm{CASPT2}} - \left({}^3\mathrm{A}\right)_{\mathrm{DFT}}\right]. \end{aligned} \quad (3)$$

As the triplet is well described by both levels of theory, we may take its relative energy difference between the DFT and CASPT2 levels to be zero. The quantity Δ provides a correction to the singlet energies produced by DFT. The final electronic energies for all singlet Cu–O_2 adducts in the full model systems are then obtained by summing the DFT electronic energies for the full model systems and the Δ obtained from calculations on the corresponding simplified models.

Results and discussion

Cu(I) complexes

Starting from the 12 Cu(I) complexes consistent with the experimental structural data, geometry optimizations were carried out for each ligand set. Only eight of these proved to be stable and suitable for further investigation; details of these geometry-optimized structures are presented in Table 1. Of the other four potential complexes, hydrogen-bond-driven dissociation of ligands [54–56] is observed in two of the cases. That the ligands in question in these two complexes are solvent-derived suggests the complex as posed is unstable and that the associated ligand set is not viable. Constraining coordination angles and optimizing metal–ligand bond lengths avoids dissociation [54], but leads to structures significantly higher in energy compared with those with intermolecular hydrogen bonding [e.g., 8.7 kcal mol^{-1} higher in the $(N)_2(H_2O)_2$ ligand set], emphasizing the instability of the former.

The geometric parameters of the calculated Cu(I) complex with the $(N)_2(H_2O)(S)$ ligand set compare favorably with EXAFS results from both DβM [27, 28] and PHM [29, 30], which identify two nitrogen donors at approximately 1.92 Å and one sulfur donor at approximately 2.25 Å from the Cu_B(I) center. The EXAFS data from DβM suggested the presence of an additional, weakly bound N, C, or O donor at a distance of 2.56 Å from the Cu_B(I), in good agreement with the Cu–OH_2 distance of 2.579 Å in the geometry-optimized structure.

The reduced PHM catalytic core crystal structure (Fig. 1a) exhibits an $(N)_2(X)(S)$ ligand set at the Cu_B site, where X indicates a tightly bound solvent-derived ligand [10]. While the Cu–N and Cu–S distances and general coordination geometry in the computed Cu(I) complex with the $(N)_2(H_2O)(S)$ ligand set are not in conflict with the crystal structure data (Table 1), the Cu–O distances, on the other hand, differ significantly. The Cu–O distance of 1.88 Å in the crystal structure has been interpreted to imply the presence of a hydroxide rather than a H_2O ligand [57–59]. With the crystal structure being obtained at pH 5.5, however, a hydroxide ligand seems unlikely. Moreover, the computed Cu(I) complex with the $(N)_2(S)(OH)$ ligand set was found to be unstable, while Cu(I) complexes with both $(N)_2(S)(H_2O)$ and $(N)_2(S)$ ligand sets were found to be stable minima. The short Cu–O distance in the crystal structure may be the result then of a disordered solvent molecule near the Cu_B site. Calculations with a longer Cu–O distance indicate that $[Cu(N)_2(S)(H_2O)]^+$ is lower in free energy than $[Cu(N)_2(S)]^+ + H_2O$ by 1.78 kcal mol^{-1}, further supporting the premise that an aqua ligand is preferred at the reduced Cu_B site.

Trends among the Cu(I) complexes are also consistent with those observed by Carvajal et al. [54] in their study on coordination number changes at Cu(I) centers.

Table 1 Geometric details for all Cu(I) complexes stable under optimization

Ligand set	Cu–N	Cu–O	Cu–S	Coordination geometry
$(N)_3$	2.039, 2.039, 2.039	–	–	Trigonal planar
$(N)_3(OH)$	2.044, 2.303, 2.303	1.965	–	Distorted tetrahedral
$(N)_3(H_2O)$	2.022, 2.022, 2.166	2.530	–	Distorted trigonal pyramidal
$(N)_3(S)$	2.068, 2.073, 2.090	–	2.702	Trigonal pyramidal
$(N)_2(OH)$	1.928, 2.332	1.857	–	T-shaped
$(N)_2(H_2O)$	1.925, 1.925	2.495	–	T-shaped
$(N)_2(S)$	1.953, 1.962	–	2.624	T-shaped
$(N)_2(H_2O)(S)$	1.992, 1.997	2.579	2.614	Distorted tetrahedral
PHM–$(N)_2(H_2O)(S)$[a]	2.06, 2.25	1.88	2.45	Distorted tetrahedral

All bond distances are measured in angstroms.
N imidazole, *S* dimethyl sulfide, *PHM* peptidylglycine α-hydroxylating monooxygenase
[a]Data from the crystal structure for reduced PHM [10]

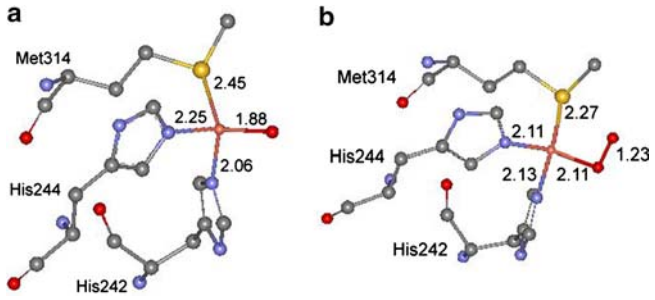

Fig. 1 Geometries of the Cu_B site in **a** the reduced peptidylglycine α-hydroxylating monooxygenase (*PHM*) catalytic core [10] and **b** the precatalytic Cu_B/O_2 PHM complex [11] crystal structures. *Pink* copper, *gray* carbon, *blue* nitrogen, *yellow* sulfur, *red* oxygen. Distances have units of angstroms

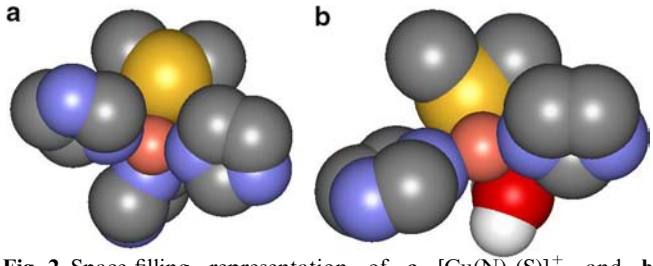

Fig. 2 Space-filling representation of **a** $[Cu(N)_3(S)]^+$ and **b** $[Cu(N)_2(H_2O)(S)]^+$, where N is imidazole and S is dimethyl sulfide. Hydrogen atoms, with the exception of those on the aqua ligand, are omitted for clarity. *Pink* copper, *gray* carbon, *blue* nitrogen, *yellow* sulfur, *red* oxygen, *white* H

When the coordination number is increased by the addition of an imidazole ligand [e.g., from $(N)_2(S)$ to $(N)_3(S)$], metal–ligand bond distances accordingly increase by approximately 0.1 Å. The variety of stable three- and four-coordinate Cu(I) complexes in Table 1 may be attributed to the relative energetic ease with which Cu(I) can accommodate third and fourth ligands in its coordination sphere [54].

1:1 $Cu–O_2$ adducts

1:1 $Cu–O_2$ adducts with each of the eight ligand sets which yielded stable Cu(I) complexes were optimized as singlets and triplets with both end-on and side-on coordination of dioxygen to the Cu center. The binding free energies (i.e., the free-energy changes for the reaction $LCu + O_2 \rightarrow LCuO_2$) at 25 °C and O–O and Cu–S bond distances for those 1:1 adducts are given in Table 2. O–O stretching frequencies in the complexes have been computed (Table S1) and are found to correlate linearly with O–O bond distances (Fig. S1), as has been seen in other computations on 1:1 metal complexes of O_2 [60].

Ligand trends

Examination of the structures in Table 2 and noting those complexes which proved unstable indicates the following trends associated with the different ligand sets. Side-on coordination of dioxygen represents a stable energetic minimum only for those cases which contain at most three ligands. Steric crowding deters side-on binding of O_2 with the four-ligand sets. The Cu(I) complexes with $(N)_3(S)$ and $(N)_2(H_2O)(S)$, for example, clearly have limited space in which to accommodate two additional bonds to Cu from dioxygen (Fig. 2). In addition, oxidized Cu(II), with a d^9 configuration, should exhibit a tetragonal distortion of the octahedral

Table 2 Binding free energies (ΔG^o, kcal mol^{-1}) at 25 °C and selected bond distances (Å) for all stable 1:1 $Cu–O_2$ adducts

Ligand set	O_2 hapticity	Multiplicity	ΔG^o	O–O	Cu–S
$(N)_2$	η^1	Singlet	(12.97)	1.244	
$(N)_3$	η^1	Singlet	4.75 (−2.70)	1.256	
	η^2	Singlet	11.35 (3.90)	1.307	
$(N)_3(OH)$	η^1	Singlet	−5.03	1.311	
	η^1	Triplet	−7.81	1.302	
$(N)_3(H_2O)$	η^1	Singlet	11.67	1.280	
	η^1	Triplet	2.48	1.226	
$(N)_3(S)$	η^1	Singlet	11.69	1.262	2.628
$(N)_2(OH)$	η^1	Singlet	2.03	1.290	
	η^2	Singlet	0.33	1.347	
	η^1	Triplet	−2.24	1.282	
	η^2	Triplet	−4.95	1.300	
$(N)_2(H_2O)$	η^1	Singlet	9.96	1.254	
	η^2	Singlet	12.97	1.321	
$(N)_2(S)$	η^1	Singlet	8.12 (9.90)	1.253	2.774
	η^2	Singlet	15.76	1.306	2.378
$(N)_2(H_2O)(S)$	η^1	Singlet	13.35	1.263	2.736
PHM–$(N)_2(S)$[a]	η^1	Singlet	(−0.50)[b]	1.23	2.27

Numbers in *parentheses* correspond to the reaction in which the Cu(I) complex included an aqua ligand
[a]From calculations based on models derived directly from available crystal structures for PHM [10, 11]
[b]Zero-point-energy correction, thermal correction to the enthalpy, and ΔS taken to be equal to those from the analogous model case

ligand field, further disfavoring coordination to the last axial site, which would have to be occupied in a six-coordinate Cu–O_2 complex. That 20-electron Cu–O_2 adducts would form from the 18-electron tetracoordinate Cu(I) complexes provides an electronic deterrent as well to dioxygen binding in these cases.

Comparing free energies of formation for adducts with differing dioxygen hapticities within ligand sets, we find that end-on coordination of dioxygen is favored over side-on coordination in all cases (by 3.0–7.6 kcal mol^{-1}). The only exception occurs for the $(N)_2(OH)$ ligand set, which has only three ligands and contains an anionic hydroxide ligand, thereby stabilizing the higher oxidation state of Cu and additional reduction of dioxygen that is associated with the increased peroxide character inherent in η^2 dioxygen coordination.

Stable equilibrium structures for triplet Cu–O_2 adducts were obtained only for the $(N)_3(H_2O)$, $(N)_3(OH)$, and $(N)_2(OH)$ ligand sets. These three most-electron-donating ligand sets support superoxide-like character in the 1:1 adduct over dioxygen-like character, which in turn stabilizes a triplet adduct over decomposition to the Cu(I) complex and molecular (triplet) oxygen. For the anionic ligand sets, the triplet complexes were 3–5 kcal mol^{-1} lower in energy than their singlet counterparts.

The anionic, hydroxide-containing ligand sets are noteworthy for their tendency to yield Cu–O_2 adducts with the lowest binding free energies and the longest O–O bond lengths. The electron-rich nature of these ligand sets is responsible for stabilizing higher oxidation states of Cu and greater reduction of the dioxygen moiety. The enhanced stability of these 1:1 adducts is a potential biological liability, however, and may result in their being relatively unreactive towards substrates, as has been seen in 1:1 Cu–O_2 adducts supported by an anionic β-diketiminate ligand [26]. The inherent stability of the hydroxide ligands themselves at the physiological pH of 7 is also low. For H_2O ligands in the Cu–O_2 complexes examined here, calculated pK_a values were essentially unchanged from that for H_2O itself.

By contrast, the neutral ligand sets provide a more biologically pertinent array of Cu–O_2 complexes. O–O bond lengths in the cases of the singlet η^1 Cu–O_2 complexes track with the net electron-donating capability of the ligand set, according to $(N)_3(H_2O) > (N)_3(S) \approx (N)_2(H_2O)(S) > (N)_3 \approx (N)_2(H_2O) \approx (N)_2(S)$. The lowest ΔG^o of formation is observed for the cases of $(N)_2(H_2O)$, $(N)_3$, and $(N)_2(S)$ (Fig. 3a–c). Other cases are somewhat less favorable, but the total spread among ΔG^o values is only 8.6 kcal mol^{-1}. The singlet end-on adducts in the $(N)_2(H_2O)$ and $(N)_3(H_2O)$ cases are stabilized by a hydrogen-bonding interaction between the aqua ligand and the superoxo moiety (Fig. 3a, d). In general, however, the trend with ΔG^o here exhibits competing effects. The four-coordinate Cu(I) complexes provide more electron density to copper, which favors dioxygen binding. This effect is offset as oxygenation of the tetracoordinate 18-electron complexes leads to the formation of 20-electron species. Additionally, coordination of the fourth ligand in the Cu(I) complex also creates a steric disincentive to dioxygen binding. Alleviation of the steric hindrance [i.e., with the $(N)_3$, $(N)_2(H_2O)$, and $(N)_2(S)$ ligand sets] and creation of 18-electron Cu–O_2 adducts from three-coordinate, 16-electron Cu(I) complexes generally leads to a more favorable ΔG^o than does maximizing the electron-donating characteristics of the ligand set [e.g., $(N)_3(S)$ and $(N)_2(H_2O)(S)$].

Correspondence to the PHM Cu_B active site

The end-on singlet Cu–O_2 adduct with the $(N)_2(S)$ ligand set has a favorable ΔG^o of formation, which is consistent with this same ligand set and dioxygen coordination mode being found at the Cu_B site (Fig. 1b) in the 1.85-Å resolution crystal structure for the PHM Cu–O_2 pre-catalytic enzyme complex [11]. The Cu–O and O–O distances are also comparable, in particular showing only slight elongation of the O–O bond as compared

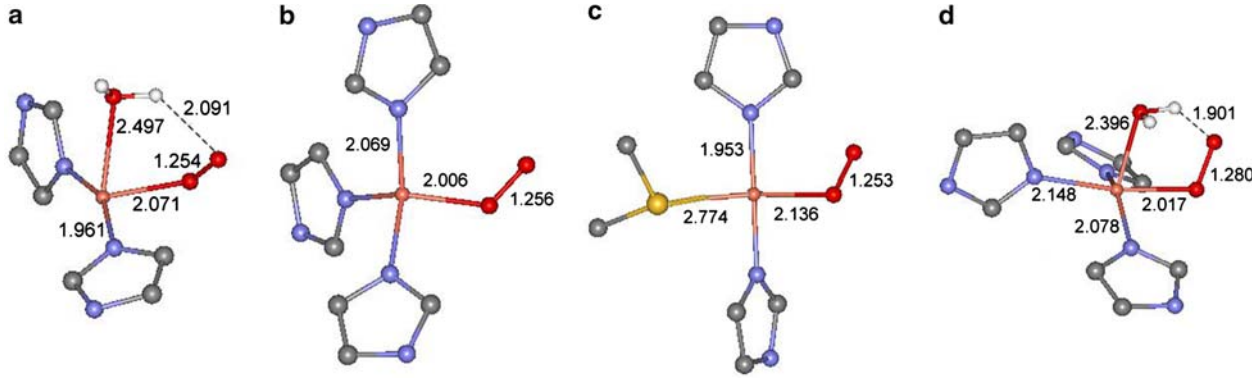

Fig. 3 Singlet end-on 1:1 Cu–O_2 adducts with the ligand sets **a** $(N)_2(H_2O)$, **b** $(N)_3$, **c** $(N)_2(S)$, and **d** $(N)_3(H_2O)$. Hydrogen atoms, with the exception of those on the aqua ligand, are omitted for clarity. *Pink* copper, *gray* carbon, *blue* nitrogen, *yellow* sulfur, *red* oxygen, *white* hydrogen. Distances have units of angstroms

with that of free molecular oxygen (1.208 Å [49]). The model complex, however, has a Cu–S distance which is 0.50 Å greater than that found in the crystal structure. Such a long and weak Cu–S interaction is similarly seen in oxidized DβM, where the Met–S is coordinated axially [28]. This difference between the model and the PHM Cu_B-site structures can be attributed to a different coordination geometry in the protein, which shows a tetrahedral coordination at Cu_B (likely due to the structural influence wrought by the protein environment), compared with the theoretical model, where dimethyl sulfide is coordinated in the equatorial position of a distorted square-planar geometry. The geometric dissimilarities between the model complex and the geometry of the PHM Cu_B site[†], however, translate into an electronic energy difference of only 1.6 kcal mol^{-1} in favor of the model system, indicating that the protein environment minimally affects the stability of the Cu–O_2 adduct. Computed η^1 Cu–O_2 complexes supported by other ligand sets exhibit similar Cu–S distances, ranging from 2.628 to 2.736 Å.

Detailed examination of the $(N)_2(S)$ singlet η^1 Cu–O_2 structure reveals that the species may be considered intermediate between a Cu(II)–superoxo and a Cu(I)–O_2 complex. The O–O bond length of 1.253 Å is longer than that in O_2, yet significantly shorter than a typical superoxo bond length of 1.35 Å. The computed ν(O–O) of 1,352 cm^{-1} is also greater than the typical values of 1,075–1,200 cm^{-1} observed for superoxo ligands [61]. Occupation numbers from the multiconfigurational CASPT2 calculations (Fig. S2) further support an electronic structure in which Cu is intermediate between d^9 and d^{10} and the dioxygen moiety is intermediate between O_2 and O_2^-. This assignment agrees well with that based on the crystal structure, which was concluded to be compatible with either dioxygen or superoxide bound to Cu [11]. There is also a strong resemblance to the transition state for oxygenation of the β-diketiminate and anilido-imine Cu(I) complexes of Tolman et al. [24] (and B.F. Gherman, W.B. Tolman, and C.J. Cramer, unpublished work), which showed weak, end-on binding of dioxygen to Cu with significant Cu(I)–O_2 character.

The possibility that the mechanism in the protein environment involves loss of a water ligand during formation of the oxygenated product is supported by calculations on both the model complexes and the crystal structure-based geometries. The free energy of oxygenation of $[Cu(N)_2(S)]^+$ is comparable to that for $[Cu(N)_2(S)(H_2O)]^+$ when the aqua ligand is released to solution upon dioxygen binding. If the aqua ligand remains bound to copper throughout, the free energy of reaction increases by 4.5 kcal mol^{-1}. Additionally, protein geometric constraints or environmental effects (either electrostatic or steric) could favor loss of a water ligand at Cu_B in PHM in the course of reaction with dioxygen. Calculations on Cu_B-site models derived directly from crystal structures [10, 11] support such a hypothesis and show that ΔG° for this reaction is -0.50 kcal mol^{-1}, which is considerably more favorable than oxygenation of the Cu(I) complex with the $(N)_2(S)$ model ligand set (Table 2). As such, PHM uses water release to drive an otherwise endergonic process, a theme which is well established in biochemistry [62–65]. Notably, the enzymatic reaction is slightly exergonic, whereas the same reaction using the model complexes, i.e., $[Cu(N)_2(S)(H_2O)]^+ + O_2 \rightarrow [Cu(N)_2(S)(O_2)]^+ + H_2O$, is endergonic by 9.90 kcal mol^{-1}. The difference can be attributed to the strain energy of 12.0 kcal mol^{-1} in the PHM $[Cu(N)_2(S)(H_2O)]^+$ structure and implies that the protein facilitates formation of the 1:1 adduct by destabilizing the reactant Cu(I) complex rather than by stabilizing the product.

Finally, we note that the calculations are consistent with the presence of hydrogen bonds to the coordinating residues His242 (to the side-chain carbonyl group of Gln272) and His244 (to the backbone carbonyl groups of Asp312 and Thr309) in both PHM crystal structures [10, 11]. Computed pK_a values for the nitrogen-based protons of the imidazole groups were high; in particular, with the $[Cu(N)_3]^+$ structure, the pK_a was 13.4. The imidazole groups should therefore remain protonated and available for hydrogen-bond donation in PHM.

The impact of such hydrogen bonding on O_2-binding free energies has been assessed for the PHM-like ligand sets $(N)_2(S)$ and $(N)_2(S)(H_2O)$ through the addition of a water molecule as a hydrogen-bond acceptor from one imidazole ring. Computed ΔG° values change by -0.55 kcal mol^{-1} for η^1 dioxygen coordination with the $(N)_2(S)$ ligand set, by -3.15 kcal mol^{-1} for the η^2 case with $(N)_2(S)$, and by -2.29 kcal mol^{-1} for the η^1 case with $(N)_2(S)(H_2O)$. While hydrogen bonding to the acceptor water molecule does lead to stabilization of the 1:1 adducts, by inducing the imidazole ligand to be more electron-donating, the relative energetic ordering of end-on versus side-on O_2 binding with the $(N)_2(S)$ ligand set remains unchanged. Given the relatively small effect created by the presence of one water molecule, the inclusion of additional water molecules or formate ions or even full deprotonation of the coordinated imidazole rings may be suggested as a means to simulate stronger hydrogen-bonding environments in the model systems. However, Cu(I) complexes in these cases proved to be unstable under optimization, preventing the computation of the corresponding dioxygen-binding free energies.

Comparison with prior calculations

Chen and Solomon [16] previously carried out calculations on PHM Cu_B active-site models which, in contrast to the results presented here, asserted the side-on bound

[†] All calculations based directly on the PHM crystal structures used models in which bonds from Cu to ligating atoms were fixed at the distances and angles present in the crystal structure (see the "Choice of model systems" section). Consequently, the main geometric parameters in these models are those shown in Fig. 1.

form to be more stable with the $(N)_2(S)$ ligand set than an end-on bound form with the $(N)_2(S)(H_2O)$ ligand set. Chen and Solomon did not report having considered an η^1 structure with the $(N)_2(S)$ ligand set. In addition, their reported side-on structure shows a surprising degree of dioxygen reduction (O–O distance of 1.387 Å; cf. Table 2). When we subjected their reported structure to geometry optimization (subject to a constraint on the locations of carbon atoms for three methyl groups that they added to mimic enzyme α carbons) at the same level of theory that they reported (unrestricted B3LYP/LANL2DZ), we found their structure not to be a stationary point, and instead its geometry relaxed smoothly to an end-on complex rather similar to those reported here. At the *restricted* B3LYP level of theory, however, their restrained structure did indeed prove to be stationary, suggesting that even if their calculation began from an unrestricted Kohn–Sham self-consistent-field solution, at some point during their optimization there was an accidental convergence to a restricted solution after which point optimization proceeded exclusively on the restricted surface. In any case, the use of uncorrected DFT energies, whether restricted or unrestricted, to assess isomer energies and reaction paths is potentially problematic, as multideterminantal character in a Cu(II)–superoxo biradical singlet state can lead to significant errors in raw DFT energies and structures [37, 66]. Thus, we believe that the crystal structure of the oxygenated PHM Cu_B site [11], which shows end-on coordination of dioxygen to copper, should be considered to be relevant and reliable, particularly given the consistency between the crystal structure and the theoretical calculations presented herein.

Based upon mixed quantum mechanics/molecular mechanics (QM/MM) calculations on DβM, Kamachi et al. [67] have also reported that end-on dioxygen coordination at the Cu_B site is energetically preferred over side-on O_2 binding. They similarly observe limited dioxygen activation by the $(N)_2(S)$ ligand set present in the Cu_B site. In particular, their lowest energy structure for the end-on Cu_B–O_2 adduct shows an O–O bond length of 1.276 Å. The increase of 0.02 Å versus the corresponding model geometry obtained in this work (Fig. 3c) is attributable to hydrogen bonding between the dioxygen moiety and bound substrate in their QM/MM structure. The favorability of these geometric results is tempered, however, by energetics computed using DFT (both RDFT and UDFT methodologies). The significant Cu(II)–superoxo character of the Cu_B–O_2 adducts has been shown to lead to considerable inaccuracies in DFT energies as a result of the multideterminantal character of this singlet biradical species [37, 66]. In the case of Kamachi et al., this leads to the unsettling result that the triplet state of the end-on adduct is the most stable, in contrast with EPR measurements which did not detect any paramagnetic species in the DβM reaction [68, 69]. The relative energies of the end-on and side-on species reported by Kamachi et al., while in qualitative agreement with the crystallographic data, are similarly quantitatively suspect. The results presented in the current work thus not only corroborate the geometric results obtained by Kamachi et al. but also importantly provide what we believe to be the first highly accurate energetic assessment of oxygenation at the Cu_B site in PHM and DβM.

Conclusions

Dioxygen binding to Cu(I) complexes supported by a variety of ligand sets consistent with spectroscopic and crystallographic data for the Cu_B site in DβM and PHM has been examined using a combination of DFT and CASPT2 methods. Calculations have shown that η^2 coordination of molecular oxygen occurs only when steric crowding around the Cu center is minimal, and that such binding is energetically preferred over η^1 coordination only when the electron-donating characteristics of the ligand set are maximized. Cases including the anionic hydroxide ligand exhibited greater reduction of the dioxygen moiety and greater exergonicity for adduct formation, but pK_a calculations indicated these complexes to be inherently unstable with respect to their protonated congeners. Among the neutral ligand sets, $(N)_2(H_2O)$, $(N)_3$, and $(N)_2(S)$ proved most favorable for dioxygen binding, with the $(N)_2(S)$ case in particular being found to be most consistent with crystal structures for PHM. The protein environment was concluded to affect the coordination geometry at Cu_B as well as the lability of aqua ligands at this site. Our results also suggest that use of a neutral ligand set in biomimetic complexes should better support η^1 dioxygen coordination, limit dioxygen reduction, and result in 1:1 adducts that are not so stable as to be unreactive with hydrocarbon substrates.

Acknowledgements We acknowledge support from the NIH through an NRSA postdoctoral fellowship to B.F.G. and from the University of Minnesota Department of Chemistry through a Gleysteen Scholarship to D.E.H. The National Science Foundation (CHE-0203346 to C.J.C.) and the NIH (GM47365 to W.B.T.) are also thanked for partial support for this work. We thank Edward Solomon and Peng Chen for stimulating discussions.

References

1. Klinman JP (1996) Chem Rev 96:2541–2561
2. Stewart LC, Klinman JP (1988) Annu Rev Biochem 57:551–592
3. Eipper BA, Stoffers DA, Mains RE (1992) Annu Rev Neurosci 15:57–85
4. Eipper BA, Milgram SL, Husten EJ, Yun HY, Mains RE (1993) Protein Sci 2:489–497
5. McMahon A, Geertman R, Sabban EL (1990) J Neurosci Res 25:395–404
6. Stoffers DA, Green CB, Eipper BA (1989) Proc Natl Acad Sci USA 86:735–739
7. Tian GC, Berry JA, Klinman JP (1994) Biochemistry 33:226–234
8. Evans JP, Ahn K, Klinman JP (2003) J Biol Chem 278:49691–49698

9. Prigge ST, Kolhekar AS, Eipper BA, Mains RE, Amzel LM (1997) Science 278:1300–1305
10. Prigge ST, Kolhekar AS, Eipper BA, Mains RE, Amzel LM (1999) Nat Struct Biol 6:976–983
11. Prigge ST, Eipper BA, Mains RE, Amzel LM (2004) Science 304:864–867
12. Solomon EI, Chen P, Metz M, Lee SK, Palmer AE (2001) Angew Chem Int Ed Engl 40:4570–4590
13. Lewis EA, Tolman WB (2004) Chem Rev 104:1047–1076
14. Mirica LM, Ottenwaelder X, Stack TDP (2004) Chem Rev 104:1013–1045
15. Chen P, Bell J, Eipper BA, Solomon EI (2004) Biochemistry 43:5735–5747
16. Chen P, Solomon EI (2004) J Am Chem Soc 126:4991–5000
17. Champloy F, Benali-Cherif N, Bruno P, Blain I, Pierrot M, Reglier M, Michalowicz A (1998) Inorg Chem 37:3910–3918
18. Santra BK, Reddy PAN, Nethaji M, Chakravarty AR (2002) Inorg Chem 41:1328–1332
19. Kodera M, Kita T, Miura I, Nakayama N, Kawata T, Kano K, Hirota S (2001) J Am Chem Soc 123:7715–7716
20. Osako T, Nagatomo S, Tachi Y, Kitagawa T, Itoh S (2002) Angew Chem Int Ed Engl 41:4325–4328
21. Fujisawa K, Tanaka M, Morooka Y, Kitajima N (1994) J Am Chem Soc 116:12079–12080
22. Chen P, Root DE, Campochiaro C, Fujisawa K, Solomon EI (2003) J Am Chem Soc 125:466–474
23. Spencer DJE, Aboelella NW, Reynolds AM, Holland PL, Tolman WB (2002) J Am Chem Soc 124:2108–2109
24. Aboelella NW, Kryatov SV, Gherman BF, Brennessel WW, Young VG Jr, Sarangi R, Rybak-Akimova EV, Hodgson KO, Hedman B, Solomon EI, Cramer CJ, Tolman WB (2004) J Am Chem Soc 126:16896–16911
25. Reynolds AM, Gherman BF, Cramer CJ, Tolman WB (2005) Inorg Chem 44:6989–6997
26. Reynolds AM, Lewis EA, Aboelella NW, Tolman WB (2005) Chem Commun 2014–2016
27. Blackburn NJ, Hasnain SS, Pettingill TM, Strange RW (1991) J Biol Chem 266:23120–23127
28. Reedy BJ, Blackburn NJ (1994) J Am Chem Soc 116:1924–1931
29. Boswell JS, Reedy BJ, Kulathila R, Merkler D, Blackburn NJ (1996) Biochemistry 35:12241–12250
30. Blackburn NJ, Rhames FC, Ralle M, Jaron S (2000) J Biol Inorg Chem 5:341–353
31. Kolhekar AS, Keutmann HT, Mains RE, Quon ASW, Eipper BA (1997) Biochemistry 36:10901–10909
32. Schrodinger LLC (2002) Jaguar 5.0. Schrodinger, Portland, OR
33. Johnson BG, Gill PMW, Pople JA (1993) J Chem Phys 98:5612–5626
34. Becke AD (1993) J Chem Phys 98:1372–1377
35. Lee CT, Yang WT, Parr RG (1988) Phys Rev B 37:785–789
36. Ducere J-M, Goursot A, Berthomieu D (2005) J Phys Chem A 109:400–408
37. Gherman BF, Cramer CJ (2004) Inorg Chem 43:7281–7283
38. Hay PJ, Wadt WR (1985) J Chem Phys 82:270–283
39. Wadt WR, Hay PJ (1985) J Chem Phys 82:284–298
40. Hay PJ, Wadt WR (1985) J Chem Phys 82:299–310
41. Bauschlicher CW, Partridge H (1995) J Chem Phys 103:1788–1791
42. Cramer CJ (2004) Essentials of computational chemistry. Theories and models, 2nd edn. Wiley, Chichester
43. Abraham MH, Andonian-Haftvan J, Whiting GS, Leo A, Taft RS (1994) J Chem Soc Perkin Trans 2 1777–1791
44. Thompson JD, Cramer CJ, Truhlar DG (2005) Theor Chem Acc 113:107–131
45. Marten B, Kim K, Cortis C, Friesner RA, Murphy RB, Ringnalda MN, Sitkoff D, Honig B (1996) J Phys Chem 100:11775–11788
46. Tannor DJ, Marten B, Murphy R, Friesner RA, Sitkoff D, Nicholls A, Ringnalda M, Goddard WA, Honig B (1994) J Am Chem Soc 116:11875–11882
47. Tissandier MD, Cowen KA, Feng WY, Gundlach E, Cohen MH, Earhart AD, Coe JV, Tuttle TR (1998) J Phys Chem A 102:7787–7794
48. Ross S (1985) The proton, applications to organic chemistry. Academic, Orlando
49. Lide DR (2004) Handbook of chemistry and physics, 85th edn. CRC, Boca Raton
50. Andersson K, Malmqvist PA, Roos BO (1992) J Chem Phys 96:1218–1226
51. Karlstrom G, Lindh R, Malmqvist PA, Roos BO, Ryde U, Veryazov V, Widmark PO, Cossi M, Schimmelpfennig B, Neograd y P, Seijo L (2003) Comput Math Sci 28:222–239
52. Barandiaran Z, Seijo L (1992) Can J Chem 70:409–415
53. Pierloot K, Dumez B, Widmark PO, Roos BO (1995) Theor Chim Acta 90:87–114
54. Carvajal MA, Novoa JJ, Alvarez S (2004) J Am Chem Soc 126:1465–1477
55. Fox BS, Beyer MK, Bondybey VE (2002) J Am Chem Soc 124:13613–13623
56. Schmiedekamp AM, Ryan MD, Deeth RJ (2002) Inorg Chem 41:5733–5743
57. Feller D, Glendening ED, de Jong WA (1999) J Chem Phys 110:1475–1491
58. Burda JV, Pavelka M, Simanek M (2004) THEOCHEM 683:183–193
59. Pavelka M, Burda JV (2005) Chem Phys 312:193–204
60. Cramer CJ, Tolman WB, Theopold KH, Rheingold AL (2003) Proc Natl Acad Sci USA 100:3635–3640
61. Vaska L (1976) Acc Chem Res 9:175–183
62. Record MT Jr, Anderson CF, Mills P, Mossing M, Roe JH (1985) Adv Biophys 20:109–135
63. von Hippel PH (1994) Science 263:769–770
64. Spolar RS, Record MT Jr (1994) Science 263:777–784
65. Dixit SB, Jayaram B (1998) J Biomol Struct Dyn 16:237–242
66. Kinsinger CR, Gherman BF, Gagliardi L, Cramer CJ (2005) J Biol Inorg Chem 10:778–789
67. Kamachi T, Kihara N, Shiota Y, Yoshizawa K (2005) Inorg Chem 44:4226–4236
68. McCracken J, Desai PR, Papadopoulos NJ, Villafranca JJ, Peisach J (1988) Biochemistry 27:4133–4137
69. Brenner MC, Klinman JP (1989) Biochemistry 28:4664–4670